STUDY OF P(VDF-*CO*-HFP)-IONIC LIQUID BASED IONOGELS FOR DESIGNING FLEXIBLE DISPLAYS

Sara Santiago,[a] Xavier Muñoz-Berbel,[b] and Gonzalo Guirado*[a]

[a] Departament de Química, Universitat Autònoma de Barcelona, Bellaterra (Barcelona), 08193, Spain. E-mail: Gonzalo.Guirado@uab.cat

[b] Instituto de Microelectrónica de Barcelona (IMB-CNM, CSIC), Bellaterra (Barcelona), 08193, Spain

ABSTRACT

In flexible displays, solid electrolytes promote electron-transfer without compromising system integrity. Ionogels (IGs) are now preferred among other solid electrolytes, e.g. inorganic and hydrogel electrolytes, for being easier to produce than the former and showing excellent properties, including high ionic conductivities, broad electrochemical window, transparency, flexibility, and non-solvent volatility than the latter. IG properties widely depend on the composition and concentration of the ionic liquid (IL) in the polymeric matrix, affecting its transparency, integrity and flexibility. Here, we have investigated the loading and composition of the IL to produce P(VDF-*co*-HFP)-based IGs to be employed as substrates in the development of flexible photo-electrochromic displays. Single IG layers of P(VDF-*co*-HFP) loaded with 79% wt. of N_{1114} TFSI were optimal among the IGs formulations, reaching conductivity values up to 1.06 $mS \cdot cm^{-1}$, showing high transparency (83 % transmittance) and a large electrochemical window (3.2 V), while maintaining flexibility and integrity. The doping of the IG with the photo-electrochromic molecule spiropyran resulted in flexible displays with fast and reversible

electrochromic and photochromic dynamics, not affecting the conformational changes of the molecule. These flexible photo-electrochromic displays, due to its simplicity, high-performance and low cost, are foreseen to impact in several fields, including smart windows, smart clothing or gas sensors, among others.

KEYWORDS

Ionic liquids • Ionogel • Flexible device •Photoelectrochromic devices •

INTRODUCTION

Ionogels (IGs) are gel electrolytes with a liquid phase consisting of an ionic liquid (IL) that percolates the solid polymeric phase. These materials are now a first choice in the development of smart electrochemical devices for combining mechanical strength, durability, flexibility, elasticity and high ionic conductivities, something impossible to attain with stiff and brittle inorganic solid-state electrolytes or hydrogels susceptible to dehydration. [1–12] Especially remarkable is the application of IGs in electro-optic devices, e.g. advanced flexible displays, where their high transparency and ionic conductivities [13–16] is combined with their excellent mechanical features, i.e. flexibility and elasticity [17–20]. For this reason, the formulation of new IGs is still a reason for the continuous study, as their electrochemical and mechanical properties are entirely related to the chemical nature of the polymer matrix and the IL. In such formulation, the choice of a suitable polymer composition with the desired properties is crucial in the gel polymer electrolyte development [2,9,21–25]. Poly(vinylidene fluoride-*co*-hexafluoropropylene) (P(VDF-*co*-HFP)) polymers are now preferred due to their high thermal and chemical stability, flexibility, and large dielectric constants, which improve ionic dissociation [26–

[28]. Additionally, HFP units reduce polymer crystallinity while enhancing ionic conductivity [29–31]. However, ionic conductivities of such polymers are normally well below the 10^{-3} and 10^{-4} S/cm [32–35] required in conventional high-voltage electrochromic devices [36–38]. The introduction of IL as ionic charge in the P(VDF-*co*-HFP) formulation increases its ionic conductivity and expands the electrochemical windows of the material, much beyond traditional solid-gel electrolytes.

In previous reports, electrochromic molecules, such as bipyridinium salts, have been incorporated in IG electrolytes to produce flexible displays [14,15,32] in a single-step fabrication process, enabling large-scale production [39]. However, the influence of IGs composition in the design, fabrication, and performance of such devices is still controversial, and there are not general tips for a function-specific design.

This work presents an exhaustive study on P(VDF-*co*-HFP)-ionic liquid-based IG composition, and its influence on opto-electrochemical performance and mechanical properties. Several IG membranes at different IL loadings and modifications of the cation and/or the anion components were prepared and studied for optimization. Finally, the optimal material was employed in the development of an photo-electrochromic display, as proof-of-concept, namely a single electrolyte layer (IG) doped with photoelectrochromic spiropyran derivatives with a wide range of applications from smart windows to gas sensors [40–48]

EXPERIMENTAL

Materials

Poly(vinylidene fluoride-*co*-hexafluoropropylene) (P(VDF-*co*-HFP), $M\bar{w}$ 300000 g·mol^{-1}), 1',3'-Dihydro-1',3',3'-trimethyl-6-nitrospiro[2*H*-1-benzopyran-2,2'-(2*H*)-indole] (spiropyran, 98 %), and anhydrous acetone for HPLC (>99.9%) were purchased from Sigma-Aldrich, and used as received.

Ionic liquids (ILs), 1-butyl-3-methylimidazolium bis(trifluoromethanesulfonyl)imide (BMIM TFSI), 1-butyl-3-methylimidazolium hexafluorophosphate (BMIM PF_6), 1-butyl-3-methylimidazolium tetrafluoroborate (BMIM BF_4), butyl-methyl-ammonium bis(trifluoromethanesulfonyl)imide (N_{1114} TFSI), 1-methyl-1-propylpiperidinium bis(trifluoromethanesulfonyl)imide (PP_{13} TFSI), and 1-butyl-1-methylpyrrolidinium bis(trifluoromethanesulfonyl)imide (BMPyr TFSI) were purchased and dried with molecular sieves of 3 Å size under vacuum for 24h to ensure a water content of < 0.001%.

ITO-coated PET sheets, 60 Ω/sq resistance, were acquired from Sigma-Aldrich. Screen-Printed electrodes for electrochemical and spectroelectrochemical measurements were purchased from DropSens.

IGs preparation

IGs were prepared by stirring the desired amount of IL, P(VDF-*co*-HFP), and acetone for 24h in acetone under N_2 atmosphere at room temperature. For all IG compositions, the weight ratio P(VDF-*co*-HFP) : Acetone of 1:20 was maintained. Once the solution was completely homogeneous, the same volume was casted in a mold and dried at room temperature for 24h to ensure the total evaporation of acetone.

Photo-electrochromic display fabrication

The photo-electrochromic display was fabricated by preparing a solution containing spiropyran 2 mM and TEMPO 4 mM in BMIM TFSI. After this step, the desired volume of solution was weighed and mixed with P(VDF-*co*-HFP) (previously dissolved in acetone in 1:20 weight ratio), in order to obtain 83.3% BMIM TFSI loading. The resulting solution was casted on a glass ¿slide? and dried for 24h. A 1.5x2 cm^2 IG area was then cut and placed between two ITO-coated PET electrodes and connected to a potentiostat.

Characterization Techniques

Potentiostat CHInstrument 660E model was used to perform electrochemical impedance spectroscopy (EIS) to provide further insights into the electrochemical properties of IGs membranes. An A.C. impedance technique was used, and a small amplitude potential oscillation of 5 mV was applied in order to guarantee the measurements in the steady state, where no significant chemical changes were observed at a frequency range between 1 MHz and 1 Hz. The D.C. potential was set at open circuit potential (OCP). The resulting impedance spectra were fitted with Chi660e software, modeling the equivalent circuit model according to the physico-chemical processes that took place on the electrode surface.

Cyclic voltammetry (CV) measurements were made with the same potentiostat model in order to determine the electrochemical windows for each IG membrane. All electrochemical studies were performed using screen printed electrodes, where carbon electrodes were used as working and counter, and Ag/AgCl were used as pseudo-reference electrodes.

FTIR spectra of IG membranes were recorded using a FTIR Tensor 27 Bruker spectrophotometer, and the Specac Golden Gate accessory for the attenuated reflectance

modality (ATR) in the range of 3300 to 650 cm^{-1}. OPUS 5.5 software was used for monitoring the spectra.

Spectroelectrochemistry studies were performed using a VSP100 model potentiostat and controlled by EC-Lab V9.51 software. The potentiostat was coupled to an LV10290 Hamamatsu spectrophotometer and controlled using BioKine 32 V4.46 software.

IG film thicknesses were examined using confocal imaging as a non-contact optical 3D profiling technique using Sensofar PLuNeox Microscopy and SensoSCAN software for monitoring.

Morphological studies of IG membranes at different percentages of BMIM TFSI were carried out using a MERLIN FE-SEM Scanning Electron Microscopy at a voltage of 1.0 kV. The samples were pre-treated by coating them with gold using Precision Etching Coating System (PECS^{TM}) sputtering.

RESULTS

1. Influence of IL loading on optical and mechanical properties of IGs

In this study, the IG membranes presented in Figure 1 were prepared and studied. They contained different cation-anion compositions, IL loading, and doping agents.

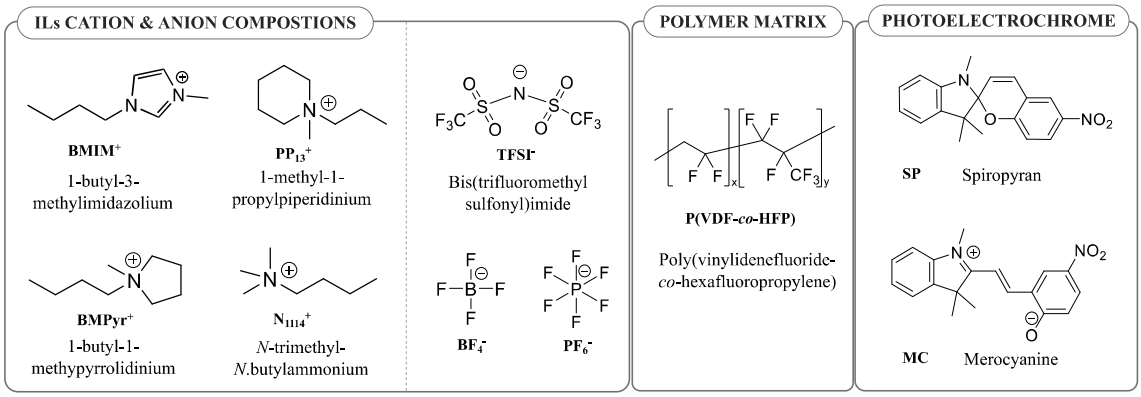

Fig. 1. Molecular structures of cation and anions of IL compositions, polymer matrix, and photoelectrochrome used in this study for IG film forming.

The effect of the IL content in the IG (weight percentage) was evaluated by loading different IL amounts in P(VDF-*co*-HFP) polymer matrices and comparing their optical, electrical and mechanical properties. The combination of $BMIM^+$ cation and $TFSI^-$ anion were used as model IL. Resulting IGs membranes presented clear aspect differences depending on the IL load (Fig. 2 **a)**), which corroborated by spectral analysis. At 50 % (weight) of BMIM TFSI or below, IG membranes were opaque, with transmittance percentages (ΔT%) in the visible range below 25% (Fig. 2 **b)**) for 40 µm-thick membranes (thickness determined by optical profilometry) and too rigid to be used in flexible displays. The optical (i.e. transparency) and rheological properties (i.e. flexibility/elasticity) of the IGs improved when increasing the percentage of IL. Maximum light transmittance was obtained when incorporating 90% of IL (ΔT% = 83%), although IG membranes lost mechanical resistance when IL concentration exceeded

86.7%. Hence, optimal IL concentration in the IG was set at 83.3% for combining excellent optical and mechanical performances.

a)

b)

Sample (% wt. BMIM TFSI)	Transmittance (%)	Conductivity (mS/cm)
0.0	14.8	-
50.0	25.4	-
70.0	50.7	0.168
75.0	56.4	0.238
80.0	63.7	0.342
83.3	71.3	0.396
86.7	76.7	0.540
90.0	83.2	1.060

Fig. 2. a) IGs prepared at different weight ratios of BMIM TFSI, showing the transparency change upon the addition of BMIM TFSI. **b)** Collected data for the change in UV-vis transmittance in the range of 400-700 nm at different loadings of BMIM TFSI and conductivity values obtained by a.c. impedance measurements.

Although IL almost completely masked the polymer network and the factual membranes morphology, SEM images revealed evident morphological changes in the IGs at high IL concentrations that influenced the optical and mechanical properties. (Fig. 3).

a)

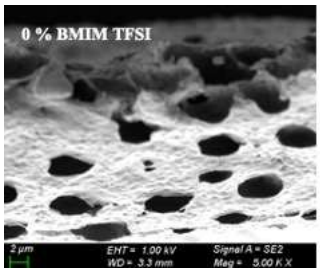

b)

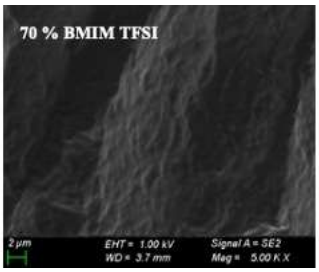

c)

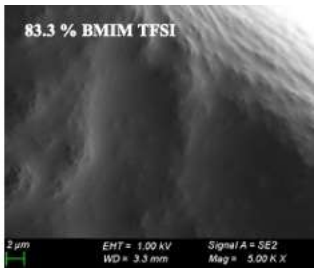

Fig. 3. Cross-sectional SEM images of **a)** pure P(VDF-*co*-HFP) (0 % BMIM TFSI) and IGs at different weight loadings of BMIM TFSI **b)** 70 % **c)** and 83.3 %.

IL apparently reduced the porosity of the membrane, which may be partially responsible for its opacity, while contributing to polymer swelling, leading to less fragile and more flexible materials. More information was obtained from FTIR spectra (Fig. 4) where pristine IL and polymer were compared to IGs. Bond vibrations corresponding to BMIM TFSI IL were observed at 1465 cm^{-1} (CH_2 scissoring bending), 1350 cm^{-1} (SO_2 antisymmetric stretching + C-SO_2-N bonding), 1229 cm^{-1} (CF vibrational stretching),

1133 cm^{-1} (SO_2 symmetric stretching), 1048 cm^{-1} (S-N-S asymmetric stretching), 792 cm^{-1} (C-S + S-N stretching), and 739 cm^{-1} (CF_3 symmetric bending + C-S stretching). On the other hand, and due to its semi-crystalline nature resulting from the folding of polymer monomers on crystalline spherulite structures [49,50], P(VDF-*co*-HFP) presented two types of vibrational modes: amorphous polar β-phase vibrations at 1404 cm^{-1} (CF_3 antisymmetric stretching), 876 cm^{-1} (CF_2 and C-C symmetric stretching) and 838 cm^{-1} (CH_2 bonding), and crystalline non-polar α-phase signals at the wavelength of 796 cm^{-1} (CF_3 stretching) and 760 cm^{-1} (CH_2 bonding). [51,52] In the IG membranes, the peaks coming from BMIM TFSI signals became more intense when increasing the IL content in the hosting P(VDF-*co*-HFP). In the case of vibrational modes associated with the polymer, those assigned to the β-phase remained present in the FTIR spectra, while those corresponding to the crystalline α-phase disappeared after addition of IL. This result suggested a change in the morphology of the P(VDF-*co*-HFP) matrix, losing part of its crystallinity and becoming more amorphous by the incorporation of IL molecules. In this sense, the addition of ILs may provoke voids or cavities among polymer chains so that spherulites were no longer formed, increasing the flexibility and elasticity of the polymer and reducing light scattering associated with these highly dispersive crystalline structures.

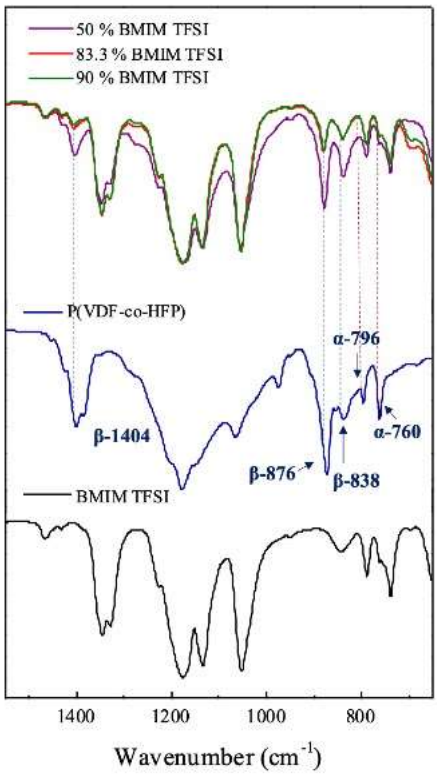

199

200 **Fig. 4.** FTIR spectra of pure BMIM TFSI, pure P(VDF-co-HFP), and IGs at different weight ratios of
201 BMIM TFSI.

202 The ionic conductivity of the IGs was determined by EIS for its direct relationship with
203 the electrochemical performance of the system. EIS spectra showed two consecutives
204 semi-circles (Fig. **5a)**) which associated to processes taking place in the electrode-
205 membrane interface and membrane, respectively. Accordingly, EIS data were fitted with
206 the equivalent circuit illustrated in Fig. 5 **b)**, containing: parasite resistance associated to
207 the contacts and the electrode material, R: the components of the electrode-IG interface
208 (R_I and C_I for the interface resistance and capacitance, respectively); and the electrical
209 parameters associated with the IG, namely the IG resistance (R_{IG}), the IG capacitance
210 (C_{IG}) and constant phase element (CPE) associated to mass transport processes in the IG
211 structure.

212

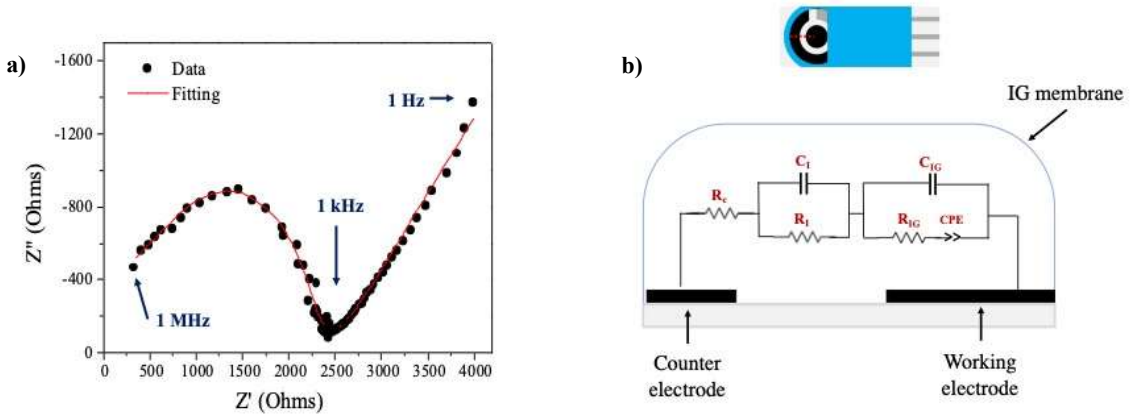

Fig. 5. a) Impedance spectra of IG at 83 % BMIM TFSI as an example of general interpretation of Nyquist plots. Experimental data in black dots and fitted impedance curve in solid red line; **b)** Equivalent circuit model for impedance spectra of IGs measured using screen-printed electrodes.

Ionic conductivity of IGs with different IL content (%wt. of BMIM TFSI; Fig. 6 **a)**) was estimated from R_{IG} impedance as detailed in previous report. [53,54]

Generally, ionic conductivity of gel electrolytes is studied by ESI using typical electrochemical cells, where the samples are sandwiched between the electrodes. However, this experimental setup directly modifies the thickness of the material affecting final conductivity values. For solving this problem, we used screen-printed electrodes, since samples are placed on the top of the electrodes. Prior use, the corresponding cell constant was calculated for this system.

Fig. 6 **b)** shows a linear decay of the inverse of the IG conductivity (resistivity) with the IL content until reaching a value of 1.05 mS/cm at 90% IL in agreement with the expected conductivity of IL solutions (3.60 mS/cm).[55] The increase of conductivity was associated to two main factors: i) the increase in the concentration of ionic species from the IL and ii) the decrease in the number of crystalline domains of P(VDF-*co*-HFP) polymer that hinder ion mobility and conductivity of the IGs. These processes, however, did not explain the high increase in conductivity observed in the samples between 86.7% and

90% of BMIM TFSI. In this case, an additional factor influenced conductivity which was the impossibility of the polymer matrix to retain more IL inside its cavities. Thus, the conductivity magnitude obtained in this last case could not be associated to the IG but to IL alone.

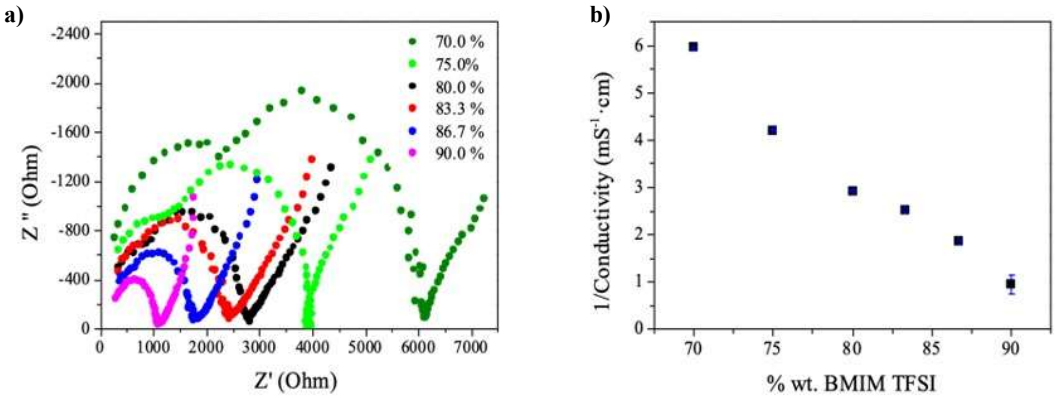

Fig. 6. a) Nyquist plot of IGs at different BMIM TFSI weight ratios. **b)** Linear relationship between the inverse of the ionic conductivity and % wt. of BMIM TFSI in IG membranes. Error bars were calculated from the standard deviation of fitted R_{IG}.

In summary, optimal IGs properties (i.e. optical, electrochemical and mechanical) were obtained after loading with 83.3% IL. This proportion was used in further optimizations of the IG formulation.

2. Influence of IL composition on optical, mechanical and electrochemical properties of IGs

The influence of the IL composition on IG properties was evaluated by combining different cation, i.e. BMIM, N_{1114}, BMPyr and PP_{13}, and anion molecules, i.e. TFSI, PF_6 and BF_4 (Fig.7 a), all containing the same molar ratio compared to IG formulated at 83.3% of BMIM TFSI. Results are summarized in Fig. 7. There was a clear correlation between optical and mechanical properties since IGs with more opacity were also qualitatively

252 more rigid and brittle. Two formulations showed a transmittance below 40% and some
253 rigidity, i.e. BMPyr TFSI and BMIM BF_4. In the first case, BMPyr may have a poorer
254 plasticizer effect than BMIM, used in the model IL, while the other cations presented
255 similar properties. The differences were more evident and reasonable when changing the
256 anion. The transparency increased with the anion size (TFSI < PF_6 < BF_4), which
257 attributed to a loss of order in the polymer chain. Qualitatively, elasticity also improved
258 along with the anion size. Large molecules incorporated in the polymeric matrix minimize
259 polymer chain interactions and the formation of crystalline structures, reducing its rigidity
260 and avoiding the formation of highly-dispersing particles responsible of polymer opacity.
261 BF_4^- was too small to produce these structural changes, resulting in opaque and rigid IGs.

262

a)

b)

Sample	Transmittance (%)	Conductivity (mS/cm)	Reduction Potential (V)	Oxidation Potential (V)	Electrochemical Window (V)
BMIM TFSI	71.3	0.396	-1.33	1.43	2.76
BMIM PF_6	69.9	0.395	-1.26	1.47	2.73
BMIM BF_4	38.4	0.846	-1.32	1.40	2.72
N_{1114} TFSI	72.8	0.303	-2.00	1.20	3.20
BMPyr TFSI	35.9	0.295	-1.73	1.20	2.93
PP_{13} TFSI	65.6	0.215	-1.73	1.10	2.83

263

264 **Fig. 7. a)** IGs prepared with IL with different cations and anions; **b)** Change in UV-vis transmittance in the
265 range of 400-700 nm using different ILs at the same molar concentration. Ionic conductivity values obtained
266 by a.c. Impedance measurements and electrochemical windows recorded by CV.

267

268 The different IL compositions also affected the electrochemical properties of the IG
269 membranes, i.e. the electrochemical window. The electrochemical window was
270 determined as the difference between the reduction and the oxidation potentials from CV
271 at the scan rate of 10 mV/s (see Fig S2 in supplementary information) that determines the
272 maximum potential range of operation of the electrochromic system.

In IGs, the electrochemical window is limited by the reduction of the cations, and the oxidation of the anions of the ILs. Large electrochemical windows between 2.7 and 3.2 V vs Ag/AgCl were obtained in all cases thanks to the electrochemical stability of the used compounds. The oxidation limits similar values than the reduction ones due to the similarly low electron-donor character of fluorinated anions responsible of the oxidation potential (TFSI, BF_4^-, PF_6^-).

Regarding reduction potentials, when substituting the quaternary amines by alkyl chains (PP_{13}, BMPyr, N_{1114}) the electrochemical reduction significantly shifted to higher values and can be attributed to a poorer electron-withdrawing effect. The combination N_{1114} TFSI provided the largest redox potentials.

Conductivity values for the different IGs formulations were obtained from the inverse of the magnitude of the R_{IG}. EIS spectra when changing anion and cation concentrations and the final conductivity magnitude are illustrated in Fig. 8. In general, all presented conductivities in the range between 0.215 mS/cm and 0.846 mS/cm, which suitable for all-solid and flexible electrochemical applications. The influence of the anion in IG conductivity was low, and only BF_4^- presented a noticeable increase in the conductivity magnitude which associated to its small size and high mobility in the IG matrix. In the case of cations, it was a clear correlation between the IG conductivity and that of the pristine ILs (BMIM > N_{1114} > BMPyr > PP_{13}). Thus, PP_{13}, the one with the largest size and less motility, presented lower conductivities.

Thus, the P(VDF-*co*-HFP)-based IG doped with 79 % IL containing N_{1114} TFSI was selected as the optimal IG formulation in the production of flexible displays for presenting the highest transparency and electrochemical window, while maintaining an acceptable conductivity. Note that 79 % of N_{1114} TFSI membranes contains same molar concentration than 83.3 % of BMIM TFSI in IG.

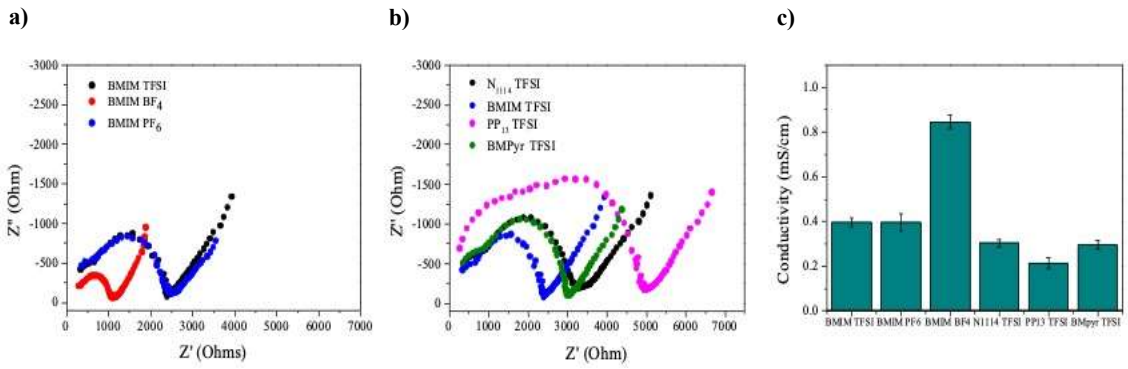

Fig. 8. Nyquist plot of the IGs when changing the **a)** anion or **b)** cation composition. **c)** Comparison of the conductivity magnitude from analysis of the previous EIS spectra. Error bars were calculated from the standard deviation of fitted R_{IG}.

3. Photo-electrochromic display fabrication

A low-cost two electrode display was prepared as a proof-of-concept by incorporating the well-known photo-electrochromic spiropyran molecule [41-44] on the previous IG. TEMPO molecule was also added as redox mediator to reduce de magnitude of the applied potential necessary to achieve the color change. To evaluate the photochromic and electrochromic capacity of the IG, it was placed between two flexible ITO-coated PET electrodes. An initial photochromic study demonstrated that spiropyran in the IG matrix responded to optical stimuli (UV light radiation) leading to the photo-isomerization from the spirocyclic form (colorless state, OFF, SP isomer) to its ring-open or merocyanine isomer (pink color, ON, MC isomer), and subsequent recovery after irradiation with visible light. Similarly, the electrochromism of the system was also explored and it was found that the application of a 2V potential in a two electrodes system (based on the standard potential of spiropyran and TEMPO, (i.e. -1.2 V and 0.80 V vs Ag/AgCl, respectively), was needed to produce the change of color in the IG from transparent to pink-orange by the reduction of SP form and the subsequent electroinduced ring-opening to the MC form (Fig 9). Mechanistically, the SP form is reduced on the cathode, leading

to formation of the open-ring radical anion, $[MC]^{-\bullet}$. Simultaneously, TEMPO was oxidized on the anode forming the corresponding cationic form, $TEMPO^{+}$. Both species, $[MC]^{-\bullet}$ and $TEMPO^{+}$, diffuse from the respective electrodes through the electrolyte layer to the bulk material. Eventually, $TEMPO^{+}$ was spontaneously regenerated due to the electron transfer reaction with $[MC]^{-\bullet}$. The oxidation of $[MC]^{-\bullet}$ after the homogenous electron transfer led to the open or merocyanine form MC, which resulted in an intense orange-pink coloration. The MC form was easily reconverted into the transparent state, SP form, upon irradiation of the material at 473 nm.

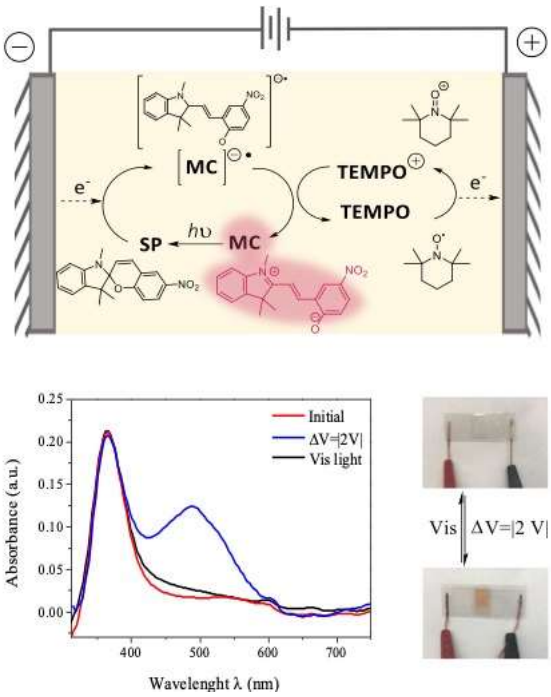

Fig. 7. a) Scheme of the electrochemical and photochemical reactions that take place in the IG membrane. **b)** UV-Vis absorbance spectra before and after the external inputs were applied **c)** Photographs for transparent, when 0 V was applied or after visible light.

CONCLUSIONS

In summary, an exhaustive study is presented on P(VDF-*co*-HFP)-IL based IGs, in which their improved formulation perfectly overcome the main issues of typical solid electrolytes for electrochemical applications and more especially for opto-electrochemical devices. Firstly, proper formulations of IGs, particularly, based on BMIM TFSI (83.3% wt.) and N_{1114} TFSI achieved high ionic conductivities, a wide electrochemical window - for higher demanding electrochemical applications- and excellent rheological properties, such as good consistency, flexibility, transparency, and elasticity. On the other hand, we demonstrated that the possibility to easily change the IL composition owing to their good chemical compatibility allows their use for further applications to be expanded.

Eventually, we demonstrated the functionality of formulated IGs, showing the performance of an opto-electrochromic device constructed following simple fabrication steps. This proof of concept served to establish and test the compatibility of improved IG formulations with the well-known spiropyran organic photoelectrochrome.

Acknowledgments

The authors thank the *Ministerio de Ciencia e Innovación* of Spain for financial support though the projects CTQ 2015-65439-R and PID2019-106171RB-I00.

REFERENCES

(1) Lodge, T. P. Materials Science: A Unique Platform for Materials Design. *Science (80-.).* **2008**, *321* (5885), 50–51. https://doi.org/10.1126/science.1159652.

(2) Le Bideau, J.; Viau, L.; Vioux, A. Ionogels, Ionic Liquid Based Hybrid Materials. *Chem. Soc. Rev.* **2011**, *40* (2), 907–925. https://doi.org/10.1039/c0cs00059k.

(3) Lai, J.; Xing, Y.; Chen, N.; Li, L.; Wu, F.; Chen, R. Electrolytes for Rechargeable Lithium–Air Batteries. *Angew. Chemie - Int. Ed.* **2019**, *59* (8), 2974–2997.

(4) Chen, N.; Zhang, H.; Li, L.; Cheng, R.; Guo, S. Ionogel Electrolytes for High-Performance Lithium Batteries: A Review. *Adv. Energy Mater.* **2018**, *8* (12), 1702675. https://doi.org/https://doi.org/10.1002/aenm.201702675.

(5) Villabona, M.; Benet, M.; Mena, S.; Al-Kaysi, R. O.; Hernando, J.; Guirado, G. Multistimuli-Responsive Fluorescent Switches Based on Spirocyclic Meisenheimer Compounds: Smart Molecules for the Design of Optical Probes and Electrochromic Materials. *J. Org. Chem.* **2018**, *83* (16), 9166–9177. https://doi.org/10.1021/acs.joc.8b01211.

(6) Sahrash, R.; Siddiqa, A.; Razzaq, H.; Iqbal, T.; Qaisar, S. PVDF Based Ionogels: Applications towards Electrochemical Devices and Membrane Separation Processes. *Heliyon* **2018**, *4* (11). https://doi.org/10.1016/j.heliyon.2018.e00847.

(7) Aller-Pellitero, M.; Santiago-Malagón, S.; Ruiz, J.; Alonso, Y.; Lakard, B.; Hihn, J. Y.; Guirado, G.; del Campo, F. J. Fully-Printed and Silicon Free Self-Powered Electrochromic Biosensors: Towards Naked Eye Quantification. *Sensors Actuators, B Chem.* **2020**, *306* (December 2019), 127535. https://doi.org/10.1016/j.snb.2019.127535.

(8) Garcia-Cortadella, R.; Schäfer, N.; Cisneros-Fernandez, J.; Re, L.; Illa, X.; Schwesig, G.; Moya, A.; Santiago, S.; Guirado, G.; Villa, R.; Sirota, A.; Serra-Graells, F.; Garrido, J. A.; Guimerà-Brunet, A. Switchless Multiplexing of Graphene Active Sensor Arrays for Brain Mapping. *Nano Lett.* **2020**, *XXXX* (XXX), XXX–XXX. https://doi.org/https://doi.org/10.1021/acs.nanolett.0c00467.

(9) MacFarlane, D. R.; Forsyth, M.; Howlett, P. C.; Kar, M.; Passerini, S.; Pringle, J. M.; Ohno, H.; Watanabe, M.; Yan, F.; Zheng, W.; Zhang, S.; Zhang, J. Ionic Liquids and Their Solid-State Analogues as Materials for Energy Generation and Storage. *Nat. Rev. Mater.* **2016**, *1* (2). https://doi.org/10.1038/natrevmats.2015.5.

(10) Salsamendi, M.; Rubatat, L.; Mecerreyes, D. Polymeric Ion Gels: Preparation Methods, Characterization, and Applications. In *Electrochemistry in Ionic Liquids*; Torriero, A. A. J., Ed.; 2015; pp 283–315. https://doi.org/10.1007/978-3-319-13485-7_9.

(11) Giffin, G. A. Ionic Liquid-Based Electrolytes for "beyond Lithium" Battery Technologies. *J. Mater. Chem. A* **2016**, *4* (35), 13378–13389. https://doi.org/10.1039/c6ta05260f.

(12) Gil-González, N.; Akyazi, T.; Zuzuarregui, A.; Castaño, E.; Benito-Lopez, F.; Morant-Miñana, M. C. Understanding the Behavior of Stimuli-Response Ionogels for Microfluidic Applications, Procedia Engineering. *Procedia Eng.* **2016**, *168*, 473–476. https://doi.org/https://doi.org/10.1016/j.proeng.2016.11.132.

(13) Chem, J. M.; Kavanagh, A.; Copperwhite, R.; Oubaha, M.; Owens, J.; Mcdonagh, C. Photo-Patternable Hybrid Ionogels for Electrochromic Applications †. *J. Mater. Chem.* **2011**, *21*, 8687–8693. https://doi.org/10.1039/c1jm10704f.

(14) Moon, H. C.; Lodge, T. P.; Frisbie, C. D. Solution-Processable

Electrochemiluminescent Ion Gels for Flexible, Low-Voltage, Emissive Displays on Plastic. *J. Am. Chem. Soc.* **2014**, *3712*. https://doi.org/10.1021/ja5002899.

(15) Moon, H. C.; Kim, C.; Lodge, T. P.; Frisbie, C. D. Multicolored , Low Power , Flexible Electrochromic Devices Based on Ion Gels. *ACS Appl. Mater. Interfaces* **2016**, *17*, 6252–6262. https://doi.org/10.1021/acsami.6b01307.

(16) Kang, M. S.; Lodge, T. P.; Gu, Y.; Zhang, S.; Lee, K. H.; Frisbie, C. D. "Cut and Stick" Rubbery Ion Gels as High Capacitance Gate Dielectrics. *Adv. Mater.* **2012**, *24* (32), 4457–4462. https://doi.org/10.1002/adma.201200950.

(17) Lodge, T. P.; Ueki, T. Mechanically Tunable, Readily Processable Ion Gels by Self-Assembly of Block Copolymers in Ionic Liquids. *Acc. Chem. Res.* **2016**, *49*, 2107–2114. https://doi.org/10.1021/acs.accounts.6b00308.

(18) Sanchez, C.; Shea, K. J.; Kitagawa, S. Hybrid Materials Themed Issue. *Chem. Soc. Rev.* **2011**, *40*, 907–925. https://doi.org/10.1039/c0cs00059k.

(19) Tang, Z.; Qi, L.; Gao, G. Structural, Thermal, and Impedance Properties of a Gel Polymer Electrolyte Containing Ionic Liquid. *Polym. Adv. Technol.* **2010**, *21*, 153–157. https://doi.org/10.1002/pat.1408.

(20) Tripathi, A. K.; Verma, Y. L.; Singh, R. K. Thermal, Electrical and Structural Studies on Ionic Liquid Confined in Ordered Mesoporous MCM-41. *J. Mater. Chem. A* **2015**, *3*, 23809–23820. https://doi.org/10.1039/c5ta05090a.

(21) Horowitz, A. I.; Panzer, M. J. Poly(Dimethylsiloxane)-Supported Ionogels with a High Ionic Liquid Loading. *Angew. Chemie Int. Ed.* **2014**, *53* (37), 9780–9783. https://doi.org/10.1002/anie.201405691.

(22) Ashby, D. S.; Ryan, H.; Block, D.; Chun-Han, L.; Christopher, S. Patternable, so-

Lution-Processed Ionogels for Thin-Film Lithium-Ion Electrolytes. *Joule* **2017**, *1* (2), 344–358. https://doi.org/https://doi.org/10.1016/j.joule.2017.08.012.

(23) Wang, X.; Zhu, H.; Greene, G. W.; Li, J.; Iranipour, N.; Garnier, C.; Fang, J.; Armand, M.; Forsyth, M.; Pringle, J. M.; Howlett, P. C. Enhancement of Ion Dynamics in Organic Ionic Plastic Crystal/PVDF Composite Electrolytes Prepared by Co-Electrospinning. *J. Mater. Chem. A* **2016**, *4* (25), 9873–9880. https://doi.org/10.1039/c6ta02817a.

(24) Li, M.; Li, J.; Nab, H.; Vlassak, J. J. Mechanical Behavior of Poly(Methyl Methacrylate)-Based Ionogels. *Soft Matter* **2014**, *10* (40), 7993. https://doi.org/https://doi.org/10.1039/C4SM01466A.

(25) Thiemann, S.; Sachnov, S. J.; Pettersson, F.; Bollström, R.; Österbacka, R.; Wasserscheid, P.; Zaumseil, J. Cellulose-Based Ionogels for Paper Electronics. *Adv. Funct. Mater.* **2013**, *24* (5), 625–634. https://doi.org/https://doi.org/10.1002/adfm.201302026.

(26) Bircan, H. et al. Use of Polymer / Ionic Liquid Plasticizers as Gel Electrolytes in Electrochromic Devices. *J. Phys. Conf. Ser.* **2008**, *127*. https://doi.org/10.1088/1742-6596/127/1/012011.

(27) Shalu; Singh, V. K.; Singh, R. K. Development of Ion Conducting Polymer Gel Electrolyte Membranes Based on Polymer PVdF-HFP, BMIMTFSI Ionic Liquid and the Li-Salt with Improved Electrical, Thermal and Structural Properties. *J. Mater. Chem. C* **2015**, *3*, 7305–7318. https://doi.org/10.1039/c5tc00940e.

(28) Abbrent, S.; Plestil, J.; Hlavata, D.; Lindgren, J.; Tegenfeldt, J.; Wendsjö, Å. Crystallinity and Morphology of PVdF-HFP-Based Gel Electrolytes. *Polymer (Guildf).* **2001**, *42*, 1407–1416. https://doi.org/10.1016/S0032-3861(00)00517-6.

(29) Zhu, Y.; Otley, M. T.; Alhashmi, F.; Kumar, A.; Zhang, X.; Mamangun, D. M. D.; Li, M.; Arden, B. G.; Sotzing, G. A. Electrochromic Properties as a Function of Electrolyte on the Performance of Electrochromic Devices Consisting of a Single-Layer Polymer. *Org. Electron.* **2014**, *15*, 1378–1386. https://doi.org/10.1016/j.orgel.2014.03.038.

(30) Tian, X.; Zhu, B.; Xu, Y. P (VDF- Co -HFP) Membrane for Recovery of Aroma Compounds from Aqueous Solutions by Pervaporation I . Ethyl Acetate / Water System. *J. Memb. Sci.* **2005**, *248*, 109–117. https://doi.org/10.1016/j.memsci.2004.10.003.

(31) Ramesh, S.; Lu, S. Effect of Lithium Salt Concentration on Crystallinity of Poly(Vinylidene Fluoride-Co-Hexafluoropropylene)-Based Solid Polymer Electrolytes. *J. Mol. Struct.* **2011**, *994*, 403–409. https://doi.org/10.1016/j.molstruc.2011.03.065.

(32) Alesanco, Y.; Miram, P.; Sebastian, D. All-in-One Gel-Based Electrochromic Devices : Strengths and Recent Developments. *Materials (Basel).* **2018**, *11*, 414. https://doi.org/10.3390/ma11030414.

(33) Sekhon, S. S.; Deepa; Agnihotry, S. A. Solvent Effect on Gel Electrolytes Containing Lithium Salts. *Solid State Ionics* **2000**, *136–137*, 1189–1192. https://doi.org/10.1016/S0167-2738(00)00584-1.

(34) Chaurasia, S. K.; Saroj, A. L.; Shalu; Singh, V. K.; Tripathi, A. K.; Gupta, A. K.; Verma, Y. L.; Singh, R. K. Studies on Structural, Thermal and AC Conductivity Scaling of PEO-LiPF6 Polymer Electrolyte with Added Ionic Liquid [BMIMPF6]. *AIP Adv.* **2015**, *5*, 077178. https://doi.org/10.1063/1.4927768.

(35) Shin, J. H.; Henderson, W. A.; Passerini, S. PEO-Based Polymer Electrolytes with

Ionic Liquids and Their Use in Lithium Metal-Polymer Electrolyte Batteries. *J. Electrochem. Soc.* **2005**, *152*, 978–983. https://doi.org/10.1149/1.1890701.

(36) Chem, J. M.; Ye, Y.; Rick, J.; Hwang, B. Ionic Liquid Polymer Electrolytes. *J. Mater. Chem. A* **2013**, *1*, 2719–2743. https://doi.org/10.1039/c2ta00126h.

(37) Fuller, J.; Breda, A. C.; Carlin, R. T. Ionic Liquid-Polymer Gel Electrolytes. *J. Electrochem. Soc.* **1997**, *144*, 8–11.

(38) Vioux, A.; Viau, L.; Volland, S.; Le, J. Use of Ionic Liquids in Sol-Gel ; Ionogels and Applications. *C.R. Chim.* **2010**, *13*, 242–255. https://doi.org/10.1016/j.crci.2009.07.002.

(39) Jensen, J.; Krebs, F. C. From the Bottom Up – Flexible Solid State Electrochromic Devices. *Adv. Mater.* **2014**, *26*, 7231–7234. https://doi.org/10.1002/adma.201402771.

(40) Stranius, K.; Börjesson, K. Determining the Photoisomerization Quantum Yield of Photoswitchable Molecules in Solution and in the Solid State. *Sci. Rep.* **2017**, *7* (December 2016), 1–9. https://doi.org/10.1038/srep41145.

(41) Kortekaas, L.; Browne, W. R. The Evolution of Spiropyran: Fundamentals and Progress of an Extraordinarily Versatile Photochrome. *Chem. Soc. Rev.* **2019**, *48* (12), 3406–3424. https://doi.org/10.1039/c9cs00203k.

(42) Preigh, M. J.; Stauffer, M. T.; Lin, F.-T.; Weber, S. G. Anodic Oxidation Mechanism of a Spiropyran. *J. Chem. Soc. Faraday Trans.* **1996**, *92* (20), 3991. https://doi.org/10.1039/ft9969203991.

(43) Ivashenko, O.; Van Herpt, J. T.; Feringa, B. L.; Rudolf, P.; Browne, W. R. Electrochemical Write and Read Functionality through Oxidative Dimerization of

Spiropyran Self-Assembled Monolayers on Gold. *J. Phys. Chem. C* **2013**, *117* (36), 18567–18577. https://doi.org/10.1021/jp406458a.

(44) Zhang, S.; Zhang, Q.; Ye, B.; Li, X.; Zhang, X.; Deng, Y. Photochromism of Spiropyran in Ionic Liquids: Enhanced Fluorescence and Delayed Thermal Reversion. *J. Phys. Chem. B* **2009**, *113* (17), 6012–6019. https://doi.org/10.1021/jp9004218.

(45) Jin Fang Zhi; Baba, R.; Hashimoto, K.; Fujishima, A. Photoelectrochromic Properties of a Spirobenzopyran Derivative. *J. Photochem. Photobiol. A Chem.* **1995**, *92* (1–2), 91–97. https://doi.org/10.1016/1010-6030(95)04167-0.

(46) Natali, M.; Giordani, S. Interaction Studies between Photochromic Spiropyrans and Transition Metal Cations: The Curious Case of Copper. *Org. Biomol. Chem.* **2012**, *10* (6), 1162–1171. https://doi.org/10.1039/c1ob06375h.

(47) Zhi, J. F.; Baba, R.; Fujishima, A. An Electrochemical Study of Some Spirobenzopyran Derivatives in Dimethylformamide. *Berichte der Bunsengesellschaft/Physical Chem. Chem. Phys.* **1996**, *100* (11), 1802–1807. https://doi.org/10.1002/bbpc.19961001108.

(48) Nam, Y. S.; Yoo, I.; Yarimaga, O.; Park, I. S.; Park, D. H.; Song, S.; Kim, J. M.; Lee, C. W. Photochromic Spiropyran-Embedded PDMS for Highly Sensitive and Tunable Optochemical Gas Sensing. *Chem. Commun.* **2014**, *50* (32), 4251–4254. https://doi.org/10.1039/c4cc00567h.

(49) Osaka, N.; Yanagi, K.; Saito, H. The Optical Transparency and Structural Change of Quenched Poly(Vinylidene Fluoride) Caused by Cold-Drawing. *Polym. J.* **2013**, *45*, 1033–1040. https://doi.org/10.1038/pj.2013.26.

(50) Ward, I. M.; Sweeney, J. *Mechanical Properties of Solid Polymers*, 3rd ed.; John Wiley & Sons, Inc, 2012.

(51) Vijayakumar, R. P.; Khakhar, D. V.; Misra, A. Phase Transformation and Enhancement of Toughness in Polyvinylidene Fluoride by Onium Salts. *J. Polym. Sci. Part B Polym. Phys.* **2011**, *49* (18), 1339–1344. https://doi.org/10.1002/polb.22303.

(52) Bormashenko, Y.; Pogreb, R.; Stanevsky, O.; Bormashenko, E. Vibrational Spectrum of PVDF and Its Interpretation. *Polym. Test.* **2004**, *23* (7), 791–796. https://doi.org/10.1016/j.polymertesting.2004.04.001.

(53) Choi, W.; Shin, H. C.; Kim, J. M.; Choi, J. Y.; Yoon, W. S. Modeling and Applications of Electrochemical Impedance Spectroscopy (Eis) for Lithium-Ion Batteries. *J. Electrochem. Sci. Technol.* **2020**, *11* (1), 1–13. https://doi.org/10.33961/jecst.2019.00528.

(54) Gil-González, N.; Akyazi, T.; Castaño, E.; Benito-Lopez, F.; Morant-Miñana, M. C. Elucidating the Role of the Ionic Liquid in the Actuation Behavior of Thermo-Responsive Ionogels. *Sensors Actuators, B Chem.* **2018**, *260*, 380–387. https://doi.org/10.1016/j.snb.2017.12.153.

(55) Stoppa, A.; Zech, O.; Kunz, W.; Buchner, R. The Conductivity of Imidazolium-Based Ionic Liquids from (-35 to 195) °c. A. Variation of Cations Alkyl Chain. *J. Chem. Eng. Data* **2010**, *55* (5), 1768–1773. https://doi.org/10.1021/je900789j.